



## 1 **Influence of biomass burning from Southeast Asia at a** 2 **high-altitude mountain receptor site in China**

3 Jing Zheng<sup>1</sup>, Min Hu<sup>1,\*</sup>, Zhuofei Du<sup>1</sup>, Dongjie Shang<sup>1</sup>, Zhaoheng Gong<sup>2,a</sup>, Yanhong  
4 Qin<sup>1</sup>, Jingyao Fang<sup>1</sup>, Fangting Gu<sup>1</sup>, Mengren Li<sup>1</sup>, Jianfei Peng<sup>1</sup>, Jie Li<sup>3</sup>, Yuqia Zhang<sup>3</sup>,  
5 Xiaofeng Huang<sup>2</sup>, Lingyan He<sup>2</sup>, Yusheng Wu<sup>1</sup>, Song Guo<sup>1</sup>

6 <sup>1</sup>State Key Joint Laboratory of Environmental Simulation and Pollution Control, College of  
7 Environmental Sciences and Engineering, Peking University, Beijing, China

8 <sup>2</sup>Key Laboratory for Urban Habitat Environmental Science and Technology, School of Environment and  
9 Energy, Peking University Shenzhen Graduate School, Shenzhen, China

10 <sup>3</sup>State Key Laboratory of Atmospheric Boundary Layer Physics and Atmospheric Chemistry (LAPC),  
11 Nansen-Zhu International Research Center (NZC), Institute of Atmospheric Physics, Chinese Academy  
12 of Sciences, Beijing, China

13 \* Correspondence to: minhu@pku.edu.cn

14 <sup>a</sup> Now at John A. Paulson School of Engineering and Applied Sciences, Harvard University, Cambridge,  
15 Massachusetts, 02138, United States

### 16 **Abstract**

17 Highly time-resolved in-situ measurements of airborne particles were made at Mt. Yulong (3410 m  
18 above sea level) on the southeastern edge of the Tibetan Plateau in China from 20 March to 14 April in  
19 2015. Detailed chemical composition was measured by a high-resolution time-of-flight aerosol mass  
20 spectrometer together with other online instruments. Average mass concentration of the submicron  
21 particles (PM<sub>1</sub>) was  $5.7 \pm 5.4 \mu\text{g m}^{-3}$  during the field campaign, ranging from  $0.1 \mu\text{g m}^{-3}$  up to  $33.3 \mu\text{g}$   
22  $\text{m}^{-3}$ . Organic aerosol (OA) was the dominant component in PM<sub>1</sub>, with a fraction of 68%. Three OA factors,  
23 i.e., biomass-burning organic aerosol (BBOA), biomass-burning-influenced oxygenated organic aerosol  
24 (OOA-BB) and oxygenated organic aerosol (OOA), were resolved using positive matrix factorization  
25 analysis. The two oxygenated OA factors accounted for 87% of the total OA mass. Three biomass burning  
26 events were identified by examining the enhancement of black carbon concentrations and the  $f_{60}$  (the  
27 ratio of the signal at  $m/z$  60 from the mass spectrum to the total signal of OA). Back trajectories of air  
28 masses and satellite fire map data were integrated to identify the biomass burning locations and pollutants  
29 transport. The western air mass from Southeast Asia with active biomass burning activities transported  
30 large amount of air pollutants, resulting in elevated organic concentrations up to 4-fold higher than that



31 of the background condition. This study at Mt. Yulong characterizes the tropospheric background  
32 aerosols of the Tibetan Plateau during pre-monsoon season, and provides clear evidence that the  
33 southeastern edge of the Tibetan Plateau is affected by transport of anthropogenic aerosols from  
34 Southeast Asia.

### 35 **1 Introduction**

36 Aerosols play an important role in the radiative balance in earth's atmosphere, with its radiative forcing  
37 still having large uncertainties (IPCC, 2013). Biomass burning emission is one of the dominant sources  
38 of atmospheric particles (von Schneidmesser et al., 2015), contributing up to 90% of the primary organic  
39 aerosol in the global scale (Bond et al., 2004) and more than half of the total organic aerosol mass in  
40 areas with significant biomass burning influences (e.g. Yangtze River Delta region in China, and Indian  
41 Peninsula) (Zhang et al., 2015; Engling and Gelencser, 2010). Given the long atmospheric lifetime of  
42 aerosols, even remote areas can sometimes be influenced by the transportation of air pollutants from  
43 areas with active biomass burnings (Bougiatioti et al., 2014). In terms of the deterioration of air quality  
44 and climate change in those remote areas, great scientific interest has arisen focusing on the impacts on  
45 biomass burning (Lau et al., 2010; Qian et al., 2011).

46 The Tibetan Plateau is the largest and highest plateau in the world, and is often regarded as the "Third  
47 Pole". It is surrounded by a ring of high-elevated mountain ranges, which were considered as blocks for  
48 transportations of air pollutants from its vicinity (Wang and French, 1994). Since this vast land has a  
49 relatively low population density with minor anthropogenic influences, the Tibetan Plateau has been  
50 considered as a natural background of the Eurasian continent (Ming et al., 2010; Wan et al., 2015). In  
51 recent years, studies have presented convincing evidences for the transport route of air pollutants  
52 climbing over the Himalayas, especially during pre-monsoon season, coinciding with the annual  
53 intensive fire season in South and Southeast Asia (Streets et al., 2003; Marinoni et al., 2010; Cong et al.,  
54 2015b). A westerly dry circulation helps to build up the smoke plume against the Himalayan ridges,  
55 elevating to 3-5 km in altitude (Bonasoni et al., 2010; Xia et al., 2011). Subsequently, downward glacier  
56 wind of local mountain breeze circulation brings biomass burning related air pollutants down to the  
57 mountain valley (Cong et al., 2015b; Lüthi et al., 2015).



58 A host of studies based on field campaigns have amassed an impressive amount of information  
59 describing the biomass burning influence on different areas of the Tibetan Plateau (Decesari et al., 2010;  
60 Zhao et al., 2013; Xu et al., 2015). Those studies were mostly approached by analyzing the temporal and  
61 spatial variations of atmospheric composition based on filter measurements. The strong correlation of  
62 carbonaceous aerosol with biomass burning tracers  $K^+$  and levoglucosan pointed out the origins of  
63 aerosols (Cong et al., 2015a). Biomass burning organic aerosol (BBOA) was also found to be a major  
64 fraction of organic aerosol (OA), with a 15% contribution to the total OA mass (Du et al., 2015). Xu et  
65 al. (2013) and You et al. (2016) also presented convincing evidences about biomass burning impacts by  
66 analyzing chemical components in glaciers collected in the Tibetan Plateau. Most of previous studies  
67 were based on offline analysis using filter or glacier samples, which were limited to low time resolution,  
68 making it difficult to follow the aging process of biomass burning aerosol. Thus in-situ measurements of  
69 aerosol chemical characterization with high time resolution are needed, so as to have a deep  
70 understanding of the sources and evolution of the particulate matter.

71 In this study, the influence of biomass burning from Southeast Asia on the Tibetan Plateau will be  
72 analyzed. The results can serve as inputs or constraints for global climate model simulations. By  
73 examining the aerosol properties as a function of chemical compositions at Mt. Yulong at the southeastern  
74 edge of the Tibetan Plateau, this study sheds light on the evolution processes of OA. Positive matrix  
75 factorization analysis was conducted to resolve different sources of OA, and characterize the influence  
76 of biomass burning from Southeast Asia transported over long distances to the Tibetan Plateau  
77 background environment during pre-monsoon season.

## 78 **2 Method**

### 79 **2.1 Site description and meteorological conditions during the campaign**

80 In this study, we conducted an intensive observation at the site on Mt. Yulong (27.2N, 100.2E), with an  
81 altitude of 3410 m a.s.l., northwestern Yunnan Province, China (Fig.1). Since Mt. Yulong is lying in the  
82 transition zone extending from the low altitudes of the Yunnan Plateau (~ 3000 a.s.l.) to the high altitude  
83 of the Tibetan Plateau (~ 5000 a.s.l.), it is on the transport route of pollutants from Southeast Asia to  
84 inland China, making it to be an ideal site to observe the influence of regional and long-range transport



85 of polluted air masses. This station is a member of the National Atmospheric Watch Network coordinated  
86 by the Chinese Environmental Monitoring Center. The famous tourist attraction Lijiang Old Town locates  
87 more than 36 km away and 1000 m lower than the elevation of the station. The observation period was  
88 conducted during the pre-monsoon season of the Tibetan Plateau, from 22 March to 14 April 2015,  
89 corresponding to the annual biomass burning seasons in Southeast Asia. Since the season was cold with  
90 sparse visitors in Lijiang old city, the influence of local emissions from residents and visitors remained  
91 low compared with other seasons.

## 92 **2.2 Measurements and data processing**

93 A high resolution time-of-flight aerosol mass spectrometer (AMS hereafter) was deployed to measure  
94 the highly time-resolved chemical composition of sub-micron, non-refractory aerosols (Table S1). The  
95 standard operation procedures of the AMS has been described in detail in Canagaratna et al. (2007).  
96 During the field operation, the AMS alternated between V and W modes, allowing the acquisitions of  
97 averaged chemical compositions of the non-refractory particles, as well as high resolution mass spectrum  
98 of organics. The detection limits (DL) of organic, sulfate, nitrate, ammonium and chloride were 0.07,  
99 0.004, 0.003, 0.005 and 0.01  $\mu\text{g m}^{-3}$ , respectively. During most time of the campaign, the mass  
100 concentrations of chloride were below its DL, and including it would lower the total signal to noise ratio,  
101 therefore it is omitted from the analysis.

102 The AMS data was analyzed using the standard AMS data analysis software, i.e., SQUIRREL (version  
103 1.57) for unit resolution mass spectrum data, and PIKA (version 1.16) for high resolution mass spectra  
104 data. Calibrations of the AMS on flow rate and ionization efficiency were conducted each week. To  
105 account for the particle loss due to the bounce of particles on the vaporizer, collection efficiencies were  
106 calculated and applied for data correction based on the method described by Middlebrook et al. (2012).

107 The high resolution organic aerosol spectra were further apportioned to different sources by positive  
108 matrix factorization (PMF) analysis (Paatero and Tapper, 1994; Ulbrich et al., 2009). The solution was  
109 validated by the characteristics of resolved mass spectra, as well as the comparison of temporal variations  
110 between each factor and external species (e.g. acetonitrile).

111 Other online instruments were also deployed at the site (Table S1). A scanning mobility particle sizer



112 (SMPS) was used to measure particle number size distribution for particle mobility diameters ranging  
113 from 3 to 780 nm, with a time resolution of 5 min. An Aethalometer was deployed to measure the aerosol  
114 light absorption coefficients  $\sigma_{ap}$  at its seven wavelengths, ranging from 370 to 950 nm. Black carbon (BC)  
115 concentration is determined by  $\sigma_{ap}$  at 880 nm using the default mass attenuation cross sections of 16.6  
116  $\text{m}^2 \text{g}^{-1}$  (Fröhlich et al., 2015). Acetonitrile was measured by a gas chromatographer with mass  
117 spectrometer and flame ionization detectors (GC–MS/FID) with a time resolution of 1 hour. Technical  
118 details of this self-made instrument were described elsewhere (Wang et al., 2016).

119 Meteorological parameters, including relative humidity, temperature, wind direction and wind speed,  
120 are continuously monitored on the site during the campaign. The low temperature ( $5^\circ\text{C}$  for the whole  
121 campaign average) and heavy snow eliminated the influence of biogenic emissions to this site during the  
122 campaign.

### 123 2.3 Back trajectory analysis and fire maps

124 To explore the influence of regional biomass burning activities on aerosol properties during the  
125 campaign, the Weather Research and Forecasting (WRF) model (version 3.61) was used to investigate  
126 the meteorological conditions and to compute trajectories of air mass arriving at Mt. Yulong. 48-h back  
127 trajectories were calculated every 6 hours from March 22 to April 14, using a starting height at 600 m  
128 above the ground level of the site.

129 Active fire points were obtained from the Fire Information for Resource Management System  
130 (FIRMS), which is provided by the Moderate Resolution Imaging Spectroradiometer (MODIS) satellite  
131 (<https://firms.modaps.eosdis.nasa.gov/firemap/>, last accessed on Aug. 26, 2016).

132

## 133 3 Results

### 134 3.1 Concentrations and chemical compositions of submicron aerosols

135 The time series of submicron aerosol compositions as well as meteorological conditions are shown in  
136 Fig.2. The average  $\text{PM}_{10}$  concentration was  $5.7 \pm 5.4 \mu\text{g m}^{-3}$ , with a range of 0.1 -  $33 \mu\text{g m}^{-3}$ . This result  
137 was similar to previous observations at the Northern Tibetan Plateau, where Du et al. (2015) reported an



138 average  $PM_{10}$  concentration of  $11.4 \mu\text{g m}^{-3}$  in the autumn of 2013, and Xu et al. (2014a) reported an annual  
139 average  $PM_{2.5}$  concentration of  $9.5 \mu\text{g m}^{-3}$  from 2006 to 2007. The averaged  $PM_{10}$  concentration was  
140 much lower than those measured at urban and downwind sites of China (e.g., (Huang et al., 2013; Xu et  
141 al., 2014b), but was three times higher than the  $1.7 \mu\text{g m}^{-3}$  at a background site in Europe in March 2004  
142 (Sjogren et al., 2008), and ten times higher than at the same background site in Europe in the spring of  
143 2013 (Fröhlich et al., 2015). These huge differences indicate that anthropogenic pollutions in Southeast  
144 Asia may have resulted in the elevation of aerosol concentrations to levels above the natural background  
145 level.

146 Averaged aerosol composition of  $PM_{10}$  is shown in the pie chart (Fig.3(a)). The  $PM_{10}$  chemical  
147 composition was dominated by organic components, which accounted for 68%, followed by sulfate  
148 (14%). The minor contribution of nitrate to  $PM_{10}$  (4%) can be explained by the lack of nearby  
149 anthropogenic sources for precursors (e.g., HONO,  $N_2O_5$ ) (Du et al., 2015). This result presents a similar  
150 picture as those observed at remote sites in the northern hemisphere (Zhang et al., 2011), as well as at a  
151 high altitude site in Europe (Ripoll et al., 2015). Compared with urban or regional areas in China, where  
152 secondary inorganic species including sulfate, nitrate and ammonium typically contribute to over one  
153 half of the total mass concentrations, the result at this site is quite unique (Huang et al., 2010; Huang et  
154 al., 2012; Xu et al., 2014b).

155 Fig. 3(b) shows the relative contribution of major chemical components as a function of  $PM_{10}$  mass  
156 concentrations, as well as the probability density of  $PM_{10}$  mass loading.  $PM_{10}$  concentrations below  $5 \mu\text{g}$   
157  $\text{m}^{-3}$  showed highest probability (68%). The fraction of organics and BC increase slightly with the  
158 increasing of  $PM_{10}$  concentrations, showing that they were the main contributors to the pollution episode  
159 in Mt. Yulong.

160 The  $PM_{10}$  components did not show distinct diel variations, but remained relatively constant during the  
161 whole day, as shown in Fig.3(c). This is similar to the findings at the Puy-de-Dôme station in central  
162 France, and the Montsec station in western Mediterranean Basin (Freney et al., 2011; Ripoll et al., 2015).  
163 Strong long-range transport of air mass with few local emissions could blur the diel cycles, since the air-  
164 mass transportations occurred regardless of the local time of the day.



165 **3.2 Characterization of organic aerosol**

166 **3.2.1 Elemental compositions of organic aerosol**

167 The elemental composition were calculated from high resolution mass spectra of organics obtained by  
168 AMS, using the method developed by Canagaratna et al. (2015). Compared with the previous method  
169 (Aiken et al., 2007; 2008), the ratio of O/C and H/C are typically increased by 20% and 7%, respectively.  
170 Bulk OA was mainly composed of carbon and oxygen, with minor contributions from hydrogen and  
171 nitrogen, and had an average molecular formula of  $C_{1.1}H_{1.4}O_{1.1}N_{0.04}$ . The fragments of organics were  
172 grouped into five types according to the existence of C, H, O or N atoms.  $C_xH_y^+$  were only 21% of the  
173 total organic signal, while the oxygen fraction ( $C_xH_yO_z^+$ ) accounted for 68% of the total OA, which is  
174 higher than those measured at urban and downwind site (30-41%) (Huang et al., 2011; Sun et al., 2011;  
175 Hu et al., 2013). The average OM/OC and O/C ratios for the whole campaign were 2.63 and 1.11,  
176 respectively, and were similar to those measured in the north eastern region of the Tibetan Plateau  
177 (OM/OC 2.75, O/C 1.16) (Xu et al., 2015). These results are slightly higher than the elemental ratios  
178 measured at another remote site (OM/OC: 2.4, O/C: 0.9) in the eastern Mediterranean (Bougiatioti et al.,  
179 2014), probably due to the mixture of free troposphere aerosol after a long time of processing before  
180 arriving at this high altitude site. The extremely high value of OM/OC reflects the highly oxidized nature  
181 of OA in the Tibetan Plateau.

182 **3.2.2 Source apportionment of organic aerosol**

183 PMF analysis was performed to investigate the sources of OA measured at Mt. Yulong. Three factors  
184 were resolved, including a biomass burning organic aerosol (BBOA), an oxygenated biomass-burning-  
185 influenced organic aerosol (OOA-BB), and an oxygenated organic aerosol (OOA). Details of the PMF  
186 analysis can be found in the supplement. The mass spectra of the three factors are shown in Fig. 4. The  
187 time series of the three factors and an external species (acetonitrile) are plotted in Fig. 5.

188 **3.2.2.1 BBOA**

189 BBOA has been frequently identified in previous studies at urban and regional sites (Zhang et al.,  
190 2011). The mass spectrum of BBOA has a notable contribution from  $m/z$  60 (mainly  $C_2H_4O_2^+$ ,  
191 contributing 3.1% of the total mass spectra), which is from fragmentation of levoglucosan. As shown in  
192 Table 1, the mass spectrum correlates well with the samples from an aircraft measurement above a large



193 forest fire (Brito et al., 2014), and well with the samples from biomass burning simulation system in the  
194 laboratory (He et al., 2010). BBOA has an O/C ratio of 0.37, presenting a similar level to previous studies  
195 (Aiken et al., 2008; He et al., 2010). The time series of BBOA correlates very well with  $K^+$  based on filter  
196 analysis (Pearson  $R=0.95$ ). The factor was also confirmed to be BBOA by its strong correlation with  
197 acetonitrile, which is a gas phase tracer for biomass burning.

198 The average concentration of BBOA was  $0.5 \mu\text{g m}^{-3}$  for the whole campaign, accounting for 13% of  
199 the total OA mass, with a maximum contribution at 61% (Fig.6 (a)). The spikes in the time series of  
200 BBOA indicate that a fraction of BBOA was contributed by primary sources nearby, possibly occasional  
201 biomass burning activities for domestic heating and cooking. The increasing fraction of BBOA as a  
202 function of total OA concentrations points to contributions from biomass burning activities during the  
203 pollution episode (Fig.6 (b)).

#### 204 3.2.2.2 OOA-BB

205 The mass spectrum of OOA-BB factor was dominated by  $C_xH_yO_z^+$  fragments, especially org29  
206 ( $\text{CHO}^+$ ), org43 ( $\text{C}_2\text{H}_3\text{O}^+$ ) and org44 ( $\text{CO}_2^+$ ). The spectrum of OOA-BB in this study well correlated with  
207 aged BBOA obtained 3 hours downwind of a forest fire (Brito et al., 2014) (Pearson  $R=0.97$ ). It is  
208 qualitatively similar to published OOA-BB spectra from aged BB plumes in China during the harvest  
209 seasons (Zhang et al., 2015), and also presented many similarities to those of OOA2-BBOA resolved in  
210 the metropolitan area of Paris (Crippa et al., 2013).

211 The average concentration of OOA-BB was  $0.9 \mu\text{g m}^{-3}$  for the whole campaign, accounting for 22%  
212 of the total OA mass. Compared with BBOA measured near sources, OOA-BB shows a higher  
213 oxygenated degree, with an O/C of 0.85, and a lower fraction of  $m/z$  60 (0.6%), as a result of the oxidation  
214 of primary levoglucosan-type species after long periods of atmospheric processing (Jolleys et al., 2015).  
215 As the plumes originated from Southeast Asia were measured at a distance of several hundred kilometers  
216 downwind, emissions would have undergone substantial aging prior to sampling. The aging process  
217 includes both the gas-phase oxidation of semi volatile species from biomass burning sources and  
218 heterogeneous or homogeneous reactions of existing particles during long-range transport (Bougiatioti  
219 et al., 2014). The time series of OOA-BB and BBOA yield modest correlations with BC (Pearson  $R=0.62$   
220 and 0.65). If we focus on the total biomass burning related organic aerosols (OOA-BB + BBOA), the R



221 value for its correlation with BC would increase to 0.76, indicating biomass burning related OA  
222 originated from the same source as BC.

### 223 3.2.2.3 OOA

224 OOA is described as highly oxidized, aged particles formed after long-range transportation and  
225 processing. The mass spectral properties of OOA are defined by having a dominant peak at  $m/z$  44  
226 (mainly  $\text{CO}_2^+$ ) and other ions of  $\text{C}_x\text{H}_y\text{O}_z^+$ . The highly oxidized nature of OOA is also reflected by its  
227 high O/C ratio of 1.45. The mass spectrum of OOA resembles that of more oxidized OOA (MO-OOA)  
228 in Beijing well (Hu et al., 2016) (Pearson  $R=0.69$ ).

229 OOA has an average concentration of  $2.6 \mu\text{g m}^{-3}$ , accounting for 65% of the total OA mass. Unlike  
230 previous studies at urban or regional sites (Jimenez et al., 2009; Li et al., 2015; Hu et al., 2016), the time  
231 series of OOA did not agree well with that of sulfate (Pearson  $R=0.32$ ), which was also the case at the  
232 puy-de-Dome research station (1465 m a.s.l.) (Freney et al., 2011). The low Pearson correlation value  
233 can be partially explained by the extremely high concentration of OOA formed from the oxidation of  
234 organics emitted by biomass burning activities during the first week of the campaign. For the rest of  
235 campaign, the correlation value for sulfate with respect to OOA factor increases to 0.77, which is  
236 consistent with previous studies.

237 As shown in Fig. 6(a), the two OOA factors (OOA-BB and OOA) were very abundant, with a  
238 predominantly contribution of 87% to the total OA mass. This is consistent with the high oxygen level  
239 in the total OA. During 80% of the observation period, OA concentrations were lower than  $5 \mu\text{g m}^{-3}$ ,  
240 with strong contributions from secondary organic aerosols (OOA and OOA-BB) (Fig.6 (b)). This  
241 indicates that the background site was predominated by organic aerosols formed through regional  
242 transportation.

## 243 4 Discussion

### 244 4.1 Identification of biomass burning events

245 Enhanced BC concentrations were used to help identifying periods influenced by biomass burning  
246 plumes (Bougiatioti et al., 2014). The BC concentration of  $85 \text{ ng m}^{-3}$  was taken as the background  
247 concentration at this site. It is the average concentration observed in the beginning of April (1 April to 4



248 April), when the strong wind scavenged pollutants of the whole region. Back trajectory and fire maps  
249 illustrate that the dominant air mass for this period was from north India with minor biomass burning  
250 activities (see Fig.7(d)). This concentration is consistent with the two-year averaged background level  
251 measured at Southern Himalayas (Marinoni et al., 2010), and comparable to the lowest BC concentrations  
252 found over the southeastern Tibetan Plateau in the pre-monsoon season (Engling et al., 2011).

253 During the sampling period, three episodes were identified as being influenced by biomass burning,  
254 with the following criteria satisfied. It includes: (a) Back trajectory analysis shows a uniform source  
255 region; (b) Fire map shows fire spots in the region during the episode; (c) BC concentrations were higher  
256 than the background level of  $85 \text{ ng m}^{-3}$  determined above. One long-lasting and strong episode was from  
257 22 March to 30 March. The air mass arrived at the site during this period was from south part of Myanmar,  
258 and covered active biomass burning areas (see Fig.7(a)). As shown on the fire map, the site may also be  
259 influenced by wildfires in the vicinity. Two less intense events were observed on 5 - 6 April and 11 - 12  
260 April, with slightly elevated BC concentrations. During the third event (11 - 12 April), the site  
261 experienced heavy snow. The back trajectory shows that air mass to this region was transported from  
262 regions with few fire spots. The enhanced BC concentration was probably emitted by biomass burning  
263 activities nearby for domestic heating and cooking.

264 These three biomass burning events were further validated by the increase of the fraction of biomass  
265 burning tracers,  $f_{60}$ , calculated as the ratio of the signal at  $m/z$  60 to the total OA signal. During the first  
266 and second events, the average  $f_{60}$  were 0.98% and 0.61%, respectively. These values were much lower  
267 than the  $f_{60}$  of 1.4% during the third event, which was influenced by fires in the vicinity. This showed the  
268 decay of  $f_{60}$  in ambient plumes transported from sources to the receptor site. During the clean episode,  
269 the  $f_{60}$  decreased to about 0.4%, indicating minor biomass burning influence (Cubison et al., 2011).

270 The box plot (Fig.8) shows the concentrations of different chemical components of biomass burning  
271 events and background conditions. The aerosol concentrations corresponding to the background  
272 condition is highlighted by light gray. Organic aerosols use the left axis while other species use the right  
273 axis, since concentration of OA were much higher than others. Aerosols corresponding to biomass  
274 burning events were at high concentrations. The concentrations of organic aerosol during three biomass  
275 burning events were 10, 4 and 6 folders higher than that of the background condition. During the first



276 event, due to co-occurrence of biomass burning activities in the vicinity together with the long-range  
277 transport of biomass burning plume, the concentration of BC reached 14 times higher than that of the  
278 background condition. All species remained at low and sustained background concentrations during the  
279 clean episode, with an average  $PM_{10}$  concentration of  $1.2 \mu g m^{-3}$ .

#### 280 4.2 Characteristic of three Biomass burning events

281 The comparison of OA fractions of different biomass burning events is shown in Fig.9. Since the air  
282 masses arriving at Mt. Yulong during the second event was transported from active biomass burning  
283 areas in Myanmar within 48h, most of the freshly emitted BBOA were processed and transformed to  
284 more oxidized OA, with OOA and OOA-BB together accounting for 90% on average of the total organic  
285 mass. In contrast, the fraction of BBOA had strong enhancement during the third event, reaching 23%.  
286 It is consistent with the previously mentioned identification that the biomass burning plumes were mainly  
287 from residential heating nearby, which could emitted large amount of fresh BBOA.

288 The aging and/or mixing processes of different biomass burning plumes are further characterized in  
289 terms of the  $f_{44}$  vs.  $f_{60}$  triangle plot (Cubison et al., 2011).  $f_{44}$ , similarly defined to  $f_{60}$  as the ratio of the  
290 signal at  $m/z$  44 to the total OA signal, is used here as an indicator of atmospheric aging, since OA and  
291 their gas phase precursor evolve in the atmosphere by becoming increasingly oxidized with higher  $CO_2^+$   
292 fraction (Jimenez et al., 2009; Ng et al., 2010). BBOA can be clearly distinguished from oxidized OA in  
293 the triangle plot. With the aging process of biomass burning plumes, OA evolved toward higher  $f_{44}$  and  
294 lower  $f_{60}$ , and gained more similar signature with OOA.

295 The OA clusters of three biomass burning events are shown clearly in the  $f_{44}$ - $f_{60}$  triangle plot (Fig.10).  
296 The OA clusters of the first and third events both present OA peaks with high  $f_{60}$  values, since the site  
297 was possibly influenced by residential heating in the surrounding regions during these two episodes. The  
298 OA cluster of the second event present more similar oxidative properties to OOA and OOA-BB, due to  
299 loss of biomass burning marker through aging process during transport.

#### 300 5 Conclusions

301 During the pre-monsoon season the aerosol evolution was explored at a high altitude receptor site on  
302 Mt. Yulong (3410 m a.s.l.) in the Tibetan Plateau in Southwestern China. The average concentration of



303  $PM_1$  was  $5.7 \mu\text{g m}^{-3}$ , which was far below that measured in urban and suburban as well as regional sites  
304 of China. The carbonaceous species were very abundant in  $PM_1$ , with an average contribution of 68%,  
305 followed by sulfate (14%) and BC (9%). This high altitude mountain site is suitable for tracing the  
306 influence of pollution plumes transported from the large areas of Southeast Asia.

307 Using PMF analysis, organic aerosol was resolved into three factors, BBOA, OOA-BB and OOA.  
308 OOA-BB formed after atmospheric process of BBOA during long-range transport. The two oxygenated  
309 OA factors (OOA and OOA-BB) accounted for 87% of the total OA, showing the highly oxidized nature  
310 of aerosol at the Mt. Yulong.

311 Different types of biomass burning events were identified by examining organic tracer in mass profiles  
312 and BC concentrations. The origins of biomass burning plumes were verified by analyzing the back  
313 trajectories of air mass as well as fire maps. Elevated  $PM_1$  concentrations due to the transport of air  
314 pollutants from active biomass burning areas in Southeast Asia were observed. Domestic heating  
315 activity also had interference on the background condition of Mt. Yulong.

316 This study provides clear evidence on the influence of the transport of pollutants emitted by biomass  
317 burning activity in Southeast Asia on the southeastern edge of the Tibetan Plateau in China. The chemical  
318 characteristics of aerosols observed by in situ measurement can serve as inputs for model validations of  
319 aerosol-cloud processes and long-range transports. This study also highlights the impact of  
320 anthropogenic emissions to the pristine region of the Tibetan Plateau, which may influence global climate.  
321

## 322 **Acknowledgements**

323 This study was supported by the National Natural Science Foundation of China (91544214,  
324 21190052 and 41121004) and the China Ministry of Environmental Protection's Special Funds for  
325 Scientific Research on Public Welfare (20130916). We also thank China National Environmental  
326 Monitoring Center for the support to the field campaign.

327

## 328 **References**

329 Aiken, A. C., DeCarlo, P. F., and Jimene, J. L.: Elemental Analysis of Organic Species with Electron  
330 Ionization High-Resolution Mass Spectrometry, *Anal. Chem.*, 79, 8350-8358, doi: 10.1021/ac071150w,



- 331 2007.
- 332 Aiken, A. C., Decarlo, P. F., Kroll, J. H., Worsnop, D. R., Huffman, J. A., Docherty, K. S., Ulbrich, I. M.,  
333 Mohr, C., Kimmel, J. R., Sueper, D., Sun, Y., Zhang, Q., Trimborn, A., Northway, M., Ziemann, P. J.,  
334 Canagaratna, M. R., Onasch, T. B., Alfarra, M. R., Prevot, A. S. H., Dommen, J., Duplissy, J., Metzger,  
335 A., Baltensperger, U., and Jimenez, J. L.: O/C and OM/OC Ratios of Primary, Secondary, and Ambient  
336 Organic Aerosols with High-Resolution Time-of-Flight Aerosol Mass Spectrometry, *Environ. Sci.*  
337 *Technol.*, 42, doi: 10.1021/es703009q, 2008.
- 338 Bonasoni, P., Laj, P., Marinoni, A., Sprenger, M., Angelini, F., Arduini, J., Bonafè U., Calzolari, F.,  
339 Colombo, T., Decesari, S., Di Biagio, C., di Sarra, A. G., Evangelisti, F., Duchi, R., Facchini, M. C.,  
340 Fuzzi, S., Gobbi, G. P., Maione, M., Panday, A., Roccatò, F., Sellegri, K., Venzac, H., Verza, G. P., Villani,  
341 P., Vuillermoz, E., and Cristofanelli, P.: Atmospheric Brown Clouds in the Himalayas: first two years of  
342 continuous observations at the Nepal Climate Observatory-Pyramid (5079 m), *Atmos. Chem. Phys.*, 10,  
343 7515-7531, doi: 10.5194/acp-10-7515-2010, 2010.
- 344 Bougiatioti, A., Stavroulas, I., Kostenidou, E., Zarpas, P., Theodosi, C., Kouvarakis, G., Canonaco, F.,  
345 Prévôt, A. S. H., Nenes, A., Pandis, S. N., and Mihalopoulos, N.: Processing of biomass-burning aerosol  
346 in the eastern Mediterranean during summertime, *Atmos. Chem. Phys.*, 14, 4793-4807, doi: 10.5194/acp-  
347 14-4793-2014, 2014.
- 348 Brito, J., Rizzo, L. V., Morgan, W. T., Coe, H., Johnson, B., Haywood, J., Longo, K., Freitas, S., Andreae,  
349 M. O., and Artaxo, P.: Ground-based aerosol characterization during the South American Biomass  
350 Burning Analysis (SAMBBA) field experiment, *Atmos. Chem. Phys.*, 14, 12069-12083, doi:  
351 10.5194/acp-14-12069-2014, 2014.
- 352 Canagaratna, M. R., Jayne, J. T., Jimenez, J. L., Allan, J. D., Alfarra, M. R., Zhang, Q., Onasch, T. B.,  
353 Drewnick, F., Coe, H., Middlebrook, A., Delia, A., Williams, L. R., Trimborn, A. M., Northway, M. J.,  
354 DeCarlo, P. F., Kolb, C. E., Davidovits, P., and Worsnop, D. R.: Chemical and microphysical  
355 characterization of ambient aerosols with the aerodyne aerosol mass spectrometer, *Mass Spectrom. Rev.*,  
356 26, 185-222, doi: 10.1002/mas.20115, 2007.
- 357 Canagaratna, M. R., Jimenez, J. L., Kroll, J. H., Chen, Q., Kessler, S. H., Massoli, P., Ruiz, L. H., Fortner,  
358 E., R. Williams, L., R. Wilson, K., Surratt, J. D., Donahue, N. M., Jayne, J. T., and R. Worsnop, D.:  
359 Elemental ratio measurements of organic compounds using aerosol mass spectrometry: characterization,  
360 improved calibration, and implications, *Atmos. Chem. Phys.*, 15, 253-272, doi: 10.5194/acp-15-253-  
361 2015, 2015.
- 362 Cong, Z., Kang, S., Kawamura, K., Liu, B., Wan, X., Wang, Z., Gao, S., and Fu, P.: Carbonaceous  
363 aerosols on the south edge of the Tibetan Plateau: concentrations, seasonality and sources, *Atmos. Chem.*  
364 *Phys.*, 15, 1573-1584, doi: 10.5194/acp-15-1573-2015, 2015a.
- 365 Cong, Z., Kawamura, K., Kang, S., and Fu, P.: Penetration of biomass-burning emissions from South  
366 Asia through the Himalayas: new insights from atmospheric organic acids, *Sci. Rep.*, 5, 9580, doi:  
367 10.1038/srep09580, 2015b.
- 368 Crippa, M., DeCarlo, P. F., Slowik, J. G., Mohr, C., Heringa, M. F., Chirico, R., Poulain, L., Freutel, F.,  
369 Sciare, J., Cozic, J., Di Marco, C. F., Elsasser, M., Nicolas, J. B., Marchand, N., Abidi, E., Wiedensohler,  
370 A., Drewnick, F., Schneider, J., Borrmann, S., Nemitz, E., Zimmermann, R., Jaffrezo, J. L., Prevot, A. S.  
371 H., and Baltensperger, U.: Wintertime aerosol chemical composition and source apportionment of the  
372 organic fraction in the metropolitan area of Paris, *Atmos. Chem. Phys.*, 13, 961-981, doi: 10.5194/acp-



- 373 13-961-2013, 2013.
- 374 Cubison, M. J., Ortega, A. M., Hayes, P. L., Farmer, D. K., Day, D., Lechner, M. J., Brune, W. H., Apel,  
375 E., Diskin, G. S., Fisher, J. A., Fuelberg, H. E., Hecobian, A., Knapp, D. J., Mikoviny, T., Riemer, D.,  
376 Sachse, G. W., Sessions, W., Weber, R. J., Weinheimer, A. J., Wisthaler, A., and Jimenez, J. L.: Effects  
377 of aging on organic aerosol from open biomass burning smoke in aircraft and laboratory studies, *Atmos.*  
378 *Chem. Phys.*, 11, 12049-12064, doi: 10.5194/acp-11-12049-2011, 2011.
- 379 Decesari, S., Facchini, M. C., Carbone, C., Giulianelli, L., Rinaldi, M., Finessi, E., Fuzzi, S., Marinoni,  
380 A., Cristofanelli, P., Duchi, R., Bonasoni, P., Vuillermoz, E., Cozic, J., Jaffrezo, J. L., and Laj, P.:  
381 Chemical composition of PM<sub>10</sub> and PM<sub>1</sub> at the high-altitude Himalayan station Nepal Climate  
382 Observatory-Pyramid (NCO-P) (5079 m a.s.l.), *Atmos. Chem. Phys.*, 10, 4583-4596, doi: 10.5194/acp-  
383 10-4583-2010, 2010.
- 384 Du, W., Sun, Y. L., Xu, Y. S., Jiang, Q., Wang, Q. Q., Yang, W., Wang, F., Bai, Z. P., Zhao, X. D., and  
385 Yang, Y. C.: Chemical characterization of submicron aerosol and particle growth events at a national  
386 background site (3295 m a.s.l.) on the Tibetan Plateau, *Atmos. Chem. Phys.*, 15, 10811-10824, doi:  
387 10.5194/acp-15-10811-2015, 2015.
- 388 Engling, G., and Gelencser, A.: Atmospheric Brown Clouds: From Local Air Pollution to Climate  
389 Change, *Elements*, 6, 223-228, doi: 10.2113/gselements.6.4.223, 2010.
- 390 Engling, G., Zhang, Y.-N., Chan, C.-Y., Sang, X.-F., Lin, M., Ho, K.-F., Li, Y.-S., Lin, C.-Y., and Lee, J.  
391 J.: Characterization and sources of aerosol particles over the southeastern Tibetan Plateau during the  
392 Southeast Asia biomass-burning season, *Tellus B*, 63, 117-128, doi: 10.1111/j.1600-0889.2010.00512.x,  
393 2011.
- 394 Fröhlich, R., Cubison, M. J., Slowik, J. G., Bukowiecki, N., Canonaco, F., Croteau, P. L., Gysel, M.,  
395 Henne, S., Herrmann, E., Jayne, J. T., Steinbacher, M., Worsnop, D. R., Baltensperger, U., and Prévôt,  
396 A. S. H.: Fourteen months of on-line measurements of the non-refractory submicron aerosol at the  
397 Jungfrauoch (3580 m a.s.l.) – chemical composition, origins and organic aerosol sources, *Atmos. Chem.*  
398 *Phys.*, 15, 11373-11398, doi: 10.5194/acp-15-11373-2015, 2015.
- 399 Freney, E. J., Sellegri, K., Canonaco, F., Boulon, J., Hervo, M., Weigel, R., Pichon, J. M., Colomb, A.,  
400 Prévôt, A. S. H., and Laj, P.: Seasonal variations in aerosol particle composition at the puy-de-Dôme  
401 research station in France, *Atmos. Chem. Phys.*, 11, 13047-13059, doi: 10.5194/acp-11-13047-2011,  
402 2011.
- 403 He, L. Y., Lin, Y., Huang, X. F., Guo, S., Xue, L., Su, Q., Hu, M., Luan, S. J., and Zhang, Y. H.:  
404 Characterization of high-resolution aerosol mass spectra of primary organic aerosol emissions from  
405 Chinese cooking and biomass burning, *Atmos. Chem. Phys.*, 10, 11535-11543, doi: 10.5194/acp-10-  
406 11535-2010, 2010.
- 407 Hu, W., Hu, M., Hu, W., Jimenez, J. L., Yuan, B., Chen, W., Wang, M., Wu, Y., Chen, C., Wang, Z., Peng,  
408 J., Zeng, L., and Shao, M.: Chemical composition, sources, and aging process of submicron aerosols in  
409 Beijing: Contrast between summer and winter, *J. Geophys. Res. Atmos.*, 121, 1955-1977, doi:  
410 10.1002/2015jd024020, 2016.
- 411 Hu, W. W., Hu, M., Yuan, B., Jimenez, J. L., Tang, Q., Peng, J. F., Hu, W., Shao, M., Wang, M., Zeng, L.,  
412 M., Wu, Y. S., Gong, Z. H., Huang, X. F., and He, L. Y.: Insights on organic aerosol aging and the  
413 influence of coal combustion at a regional receptor site of central eastern China, *Atmos. Chem. Phys.*,  
414 13, 10095-10112, doi: 10.5194/acp-13-10095-2013, 2013.



- 415 Huang, X.-F., Xue, L., Tian, X.-D., Shao, W.-W., Sun, T.-L., Gong, Z.-H., Ju, W.-W., Jiang, B., Hu, M.,  
416 and He, L.-Y.: Highly time-resolved carbonaceous aerosol characterization in Yangtze River Delta of  
417 China: Composition, mixing state and secondary formation, *Atmos. Environ.*, 64, 200-207, doi:  
418 10.1016/j.atmosenv.2012.09.059, 2013.
- 419 Huang, X. F., He, L. Y., Hu, M., Canagaratna, M. R., Sun, Y., Zhang, Q., Zhu, T., Xue, L., Zeng, L. W.,  
420 Liu, X. G., Zhang, Y. H., Jayne, J. T., Ng, N. L., and Worsnop, D. R.: Highly time-resolved chemical  
421 characterization of atmospheric submicron particles during 2008 Beijing Olympic Games using an  
422 Aerodyne High-Resolution Aerosol Mass Spectrometer, *Atmos. Chem. Phys.*, 10, 8933-8945, doi:  
423 10.5194/acp-10-8933-2010, 2010.
- 424 Huang, X. F., He, L. Y., Hu, M., Canagaratna, M. R., Kroll, J. H., Ng, N. L., Zhang, Y. H., Lin, Y., Xue,  
425 L., Sun, T. L., Liu, X. G., Shao, M., Jayne, J. T., and Worsnop, D. R.: Characterization of submicron  
426 aerosols at a rural site in Pearl River Delta of China using an Aerodyne High-Resolution Aerosol Mass  
427 Spectrometer, *Atmos. Chem. Phys.*, 11, 1865-1877, doi: 10.5194/acp-11-1865-2011, 2011.
- 428 Huang, X. F., He, L. Y., Xue, L., Sun, T. L., Zeng, L. W., Gong, Z. H., Hu, M., and Zhu, T.: Highly time-  
429 resolved chemical characterization of atmospheric fine particles during 2010 Shanghai World Expo,  
430 *Atmos. Chem. Phys.*, 12, 4897-4907, doi: 10.5194/acp-12-4897-2012, 2012.
- 431 IPCC: Climate change: the physical science basis, Cambridge University Press, Cambridge, England,  
432 2013.
- 433 Jimenez, J. L., Canagaratna, M. R., Donahue, N. M., Prevot, A. S. H., Zhang, Q., Kroll, J. H., DeCarlo,  
434 P. F., Allan, J. D., Coe, H., Ng, N. L., Aiken, A. C., Docherty, K. S., Ulbrich, I. M., Grieshop, A. P.,  
435 Robinson, A. L., Duplissy, J., Smith, J. D., Wilson, K. R., Lanz, V. A., Hueglin, C., Sun, Y. L., Tian, J.,  
436 Laaksonen, A., Raatikainen, T., Rautiainen, J., Vaattovaara, P., Ehn, M., Kulmala, M., Tomlinson, J. M.,  
437 Collins, D. R., Cubison, M. J., Dunlea, J., Huffman, J. A., Onasch, T. B., Alfarra, M. R., Williams, P. I.,  
438 Bower, K., Kondo, Y., Schneider, J., Drewnick, F., Borrmann, S., Weimer, S., Demerjian, K., Salcedo,  
439 D., Cottrell, L., Griffin, R., Takami, A., Miyoshi, T., Hatakeyama, S., Shimono, A., Sun, J. Y., Zhang, Y.  
440 M., Dzepina, K., Kimmel, J. R., Sueper, D., Jayne, J. T., Herndon, S. C., Trimborn, A. M., Williams, L.  
441 R., Wood, E. C., Middlebrook, A. M., Kolb, C. E., Baltensperger, U., and Worsnop, D. R.: Evolution of  
442 Organic Aerosols in the Atmosphere, *Science*, 326, 1525-1529, doi: 10.1126/science.1180353, 2009.
- 443 Jolleys, M. D., Coe, H., McFiggans, G., Taylor, J. W., O'Shea, S. J., Breton, M. L., Bauguutte, S. J.-B.,  
444 Moller, S., Carlo, P. D., Aruffo, E., Palmer, P. I., Lee, J. D., Percival, C. J., and Gallagher, M. W.:  
445 Properties and evolution of biomass burning organic aerosol from Canadian boreal forest fire, *Atmos.*  
446 *Chem. Phys.*, 15, 3077-3095, doi: 10.5194/acp-15-3077-2015, 2015.
- 447 Lüthi, Z. L., Škerlak, B., Kim, S. W., Lauer, A., Mues, A., Rupakheti, M., and Kang, S.: Atmospheric  
448 brown clouds reach the Tibetan Plateau by crossing the Himalayas, *Atmos. Chem. Phys.*, 15, 6007-6021,  
449 doi: 10.5194/acp-15-6007-2015, 2015.
- 450 Lau, W. K. M., Kim, M.-K., Kim, K.-M., and Lee, W.-S.: Enhanced surface warming and accelerated  
451 snow melt in the Himalayas and Tibetan Plateau induced by absorbing aerosols, *Environ. Res. Lett.*, 5,  
452 025204, doi: 10.1088/1748-9326/5/2/025204, 2010.
- 453 Li, Y. J., Lee, B. P., Su, L., Fung, J. C. H., and Chan, C. K.: Seasonal characteristics of fine particulate  
454 matter (PM) based on high-resolution time-of-flight aerosol mass spectrometric HR-ToF-AMS  
455 measurements at the HKUST Supersite in Hong Kong, *Atmos. Chem. Phys.*, 15, 37-53, doi:  
456 10.5194/acp-15-37-2015, 2015.



- 457 Marinoni, A., Cristofanelli, P., Laj, P., Duchi, R., Calzolari, F., Decesari, S., Sellegri, K., Vuillermoz, E.,  
458 Verza, G. P., Villani, P., and Bonasoni, P.: Aerosol mass and black carbon concentrations, a two year  
459 record at NCO-P (5079 m, Southern Himalayas), *Atmos. Chem. Phys.*, 10, 8551-8562, doi: 10.5194/acp-  
460 10-8551-2010, 2010.
- 461 Middlebrook, A. M., Bahreini, R., Jimenez, J. L., and Canagaratna, M. R.: Evaluation of Composition-  
462 Dependent Collection Efficiencies for the Aerodyne Aerosol Mass Spectrometer using Field Data,  
463 *Aerosol Sci. Technol.*, 46, 258-271, doi: 10.1080/02786826.2011.620041, 2012.
- 464 Ming, J., Xiao, C., Sun, J., Kang, S., and Bonasoni, P.: Carbonaceous particles in the atmosphere and  
465 precipitation of the Nam Co region, central Tibet, *J. Environ. Sci.*, 22, 1748-1756, doi: 10.1016/s1001-  
466 0742(09)60315-6, 2010.
- 467 Ng, N. L., Canagaratna, M. R., Zhang, Q., Jimenez, J. L., Tian, J., Ulbrich, I. M., Kroll, J. H., Docherty,  
468 K. S., Chhabra, P. S., Bahreini, R., Murphy, S. M., Seinfeld, J. H., Hildebrandt, L., Donahue, N. M.,  
469 DeCarlo, P. F., Lanz, V. A., Prévôt, A. S. H., Dinar, E., Rudich, Y., and Worsnop, D. R.: Organic aerosol  
470 components observed in Northern Hemispheric datasets from Aerosol Mass Spectrometry, *Atmos. Chem.*  
471 *Phys.*, 10, 4625-4641, doi: 10.5194/acp-10-4625-2010, 2010.
- 472 Paatero, P., and Tapper, U.: Positive matrix factorization: A non-negative factor model with optimal  
473 utilization of error estimates of data values, *Environmetrics*, 5, 111-126, doi: 10.1002/env.3170050203,  
474 1994.
- 475 Qian, Y., Flanner, M. G., Leung, L. R., and Wang, W.: Sensitivity studies on the impacts of Tibetan  
476 Plateau snowpack pollution on the Asian hydrological cycle and monsoon climate, *Atmos. Chem. Phys.*,  
477 11, 1929-1948, doi: 10.5194/acp-11-1929-2011, 2011.
- 478 Ripoll, A., Minguillón, M. C., Pey, J., Jimenez, J. L., Day, D. A., Sosedova, Y., Canonaco, F., Prévôt, A.  
479 S. H., Querol, X., and Alastuey, A.: Long-term real-time chemical characterization of submicron aerosols  
480 at Montsec (southern Pyrenees, 1570m.a.s.l.), *Atmos. Chem. Phys.*, 15, 2935-2951, doi: 10.5194/acp-15-  
481 2935-2015, 2015.
- 482 Sjogren, S., Gysel, M., E. Weingartner, Alfarra, M. R., Duplissy, J., Cozic, J., Crosier, J., Coe, H., and  
483 Baltensperger, U.: Hygroscopicity of the submicrometer aerosol at the high-alpine site Jungfraujoch,  
484 3580m a.s.l., Switzerland, *Atmos. Chem. Phys.*, 8, 5715-5729, doi: 10.5194/acp-8-5715-2008, 2008.
- 485 Streets, D. G., Yarber, K. F., Woo, J. H., and Carmichael, G. R.: Biomass burning in Asia: Annual and  
486 seasonal estimates and atmospheric emissions, *Global Biogeochem. Cycles*, 17, 1759-1768, doi:  
487 10.1029/2003gb002040, 2003.
- 488 Sun, Y. L., Zhang, Q., Schwab, J. J., Demerjian, K. L., Chen, W. N., Bae, M. S., Hung, H. M., Hogrefe,  
489 O., Frank, B., Rattigan, O. V., and Lin, Y. C.: Characterization of the sources and processes of organic  
490 and inorganic aerosols in New York city with a high-resolution time-of-flight aerosol mass spectrometer,  
491 *Atmos. Chem. Phys.*, 11, 1581-1602, doi: 10.5194/acp-11-1581-2011, 2011.
- 492 Ulbrich, I. M., Canagaratna, M. R., Zhang, Q., Worsnop, D. R., and Jimenez, J. L.: Interpretation of  
493 organic components from Positive Matrix Factorization of aerosol mass spectrometric data, *Atmos.*  
494 *Chem. Phys.*, 9, 2891-2918, doi: 10.5194/acp-9-2891-2009, 2009.
- 495 von Schneidemesser, E., Monks, P. S., Allan, J. D., Bruhwiler, L., Forster, P., Fowler, D., Lauer, A.,  
496 Morgan, W. T., Paasonen, P., Righi, M., Sindelarova, K., and Sutton, M. A.: Chemistry and the Linkages  
497 between Air Quality and Climate Change, *Chem. Rev.*, 115, 3856-3897, doi:  
498 10.1021/acs.chemrev.5b00089, 2015.



- 499 Wan, X., Kang, S., Wang, Y., Xin, J., Liu, B., Guo, Y., Wen, T., Zhang, G., and Cong, Z.: Size distribution  
500 of carbonaceous aerosols at a high-altitude site on the central Tibetan Plateau (Nam Co Station,  
501 4730m.a.s.l.), *Atmos. Res.*, 153, 155-164, doi: 10.1016/j.atmosres.2014.08.008, 2015.
- 502 Wang, B., and French, H. M.: Climate Controls and High-Altitude Permafrost, Qinghai-Xizang (Tibet)  
503 Plateau, China, *Permafrost and Periglacial Processes*, 5, 87-100, doi: 10.1002/ppp.3430050203, 1994.
- 504 Wang, B., Liu, Y., Shao, M., Lu, S., Wang, M., Yuan, B., Gong, Z., He, L., Zeng, L., Hu, M., and Zhang,  
505 Y.: The contributions of biomass burning to primary and secondary organics: A case study in Pearl River  
506 Delta (PRD), China, *Sci. Total. Environ.*, 569-570, 548-556, doi: 10.1016/j.scitotenv.2016.06.153, 2016.
- 507 Xia, X., Zong, X., Cong, Z., Chen, H., Kang, S., and Wang, P.: Baseline continental aerosol over the  
508 central Tibetan plateau and a case study of aerosol transport from South Asia, *Atmos. Environ.*, 45, 7370-  
509 7378, doi: 10.1016/j.atmosenv.2011.07.067, 2011.
- 510 Xu, J., Zhang, Q., Li, X., Ge, X., Xiao, C., Ren, J., and Qin, D.: Dissolved organic matter and inorganic  
511 ions in a central Himalayan glacier--insights into chemical composition and atmospheric sources,  
512 *Environ. Sci. Technol.*, 47, 6181-6188, doi: 10.1021/es4009882, 2013.
- 513 Xu, J., Wang, Z., Yu, G., Qin, X., Ren, J., and Qin, D.: Characteristics of water soluble ionic species in  
514 fine particles from a high altitude site on the northern boundary of Tibetan Plateau: Mixture of mineral  
515 dust and anthropogenic aerosol, *Atmos. Res.*, 143, 43-56, doi: 10.1016/j.atmosres.2014.01.018, 2014a.
- 516 Xu, J., Zhang, Q., Chen, M., Ge, X., Ren, J., and Qin, D.: Chemical composition, sources, and processes  
517 of urban aerosols during summertime in northwest China: insights from high-resolution aerosol mass  
518 spectrometry, *Atmos. Chem. Phys.*, 14, 12593-12611, doi: 10.5194/acp-14-12593-2014, 2014b.
- 519 Xu, J. Z., Zhang, Q., Wang, Z. B., Yu, G. M., Ge, X. L., and Qin, X.: Chemical composition and size  
520 distribution of summertime PM<sub>2.5</sub> at a high altitude remote location in the northeast of the Qinghai-  
521 Xizang (Tibet) Plateau: insights into aerosol sources and processing in free troposphere, *Atmos. Chem.*  
522 *Phys.*, 15, 5069-5081, doi: 10.5194/acp-15-5069-2015, 2015.
- 523 You, C., Xu, C., Xu, B., Zhao, H., and Song, L.: Levoglucosan evidence for biomass burning records  
524 over Tibetan glaciers, *Environ. Pollu.*, 216, 173-181, doi: 10.1016/j.envpol.2016.05.074, 2016.
- 525 Zhang, Q., Jimenez, J. L., Canagaratna, M. R., Ulbrich, I. M., Ng, N. L., Worsnop, D. R., and Sun, Y.:  
526 Understanding atmospheric organic aerosols via factor analysis of aerosol mass spectrometry: a review,  
527 *Anal Bioanal Chem*, 401, 3045-3067, doi: 10.1007/s00216-011-5355-y, 2011.
- 528 Zhang, Y. J., Tang, L. L., Wang, Z., Yu, H. X., Sun, Y. L., Liu, D., Qin, W., Canonaco, F., Prévôt, A. S.  
529 H., Zhang, H. L., and Zhou, H. C.: Insights into characteristics, sources, and evolution of submicron  
530 aerosols during harvest seasons in the Yangtze River delta region, China, *Atmos. Chem. Phys.*, 15, 1331-  
531 1349, doi: 10.5194/acp-15-1331-2015, 2015.
- 532 Zhao, Z., Cao, J., Shen, Z., Xu, B., Zhu, C., Chen, L. W. A., Su, X., Liu, S., Han, Y., Wang, G., and Ho,  
533 K.: Aerosol particles at a high-altitude site on the Southeast Tibetan Plateau, China: Implications for  
534 pollution transport from South Asia, *J. Geophys. Res. Atmos*, 118, 11,360-311,375, doi:  
535 10.1002/jgrd.50599, 2013.
- 536
- 537
- 538



539

**Table1. Comparison between mass spectra of different OA with reference spectra.**

	Reference spectra	Pearson Correlation Coefficient			Citation
		BBOA	OOA-BB	OOA	
Ambient measurement	900m above fire	0.91	0.56	0.34	Brito et al. (2014)
	3h downwind	0.51	0.97	0.91	Brito et al. (2014)
	MO-OOA	0.69	0.86	0.69	Hu et al. (2016)
	BBOA	0.85	0.38	0.11	Hu et al. (2016)
Laboratory simulation	wood of pin	0.91	0.61	0.42	He et al. (2010)
	rice straw	0.94	0.6	0.36	He et al. (2010)

540

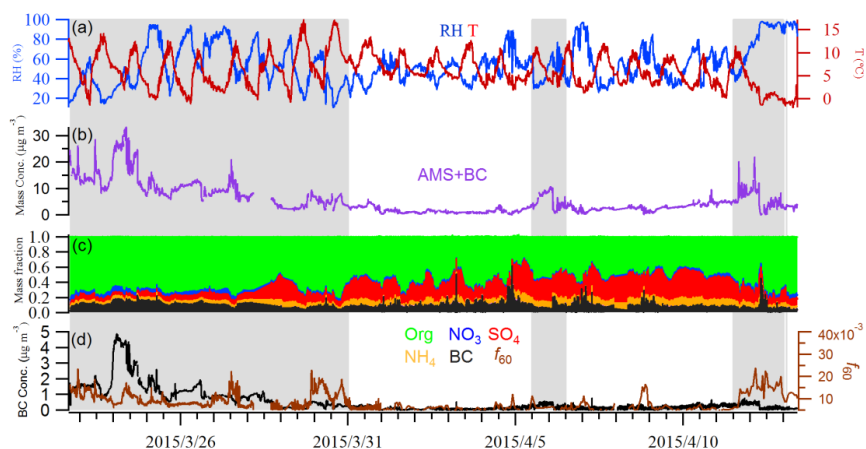
541



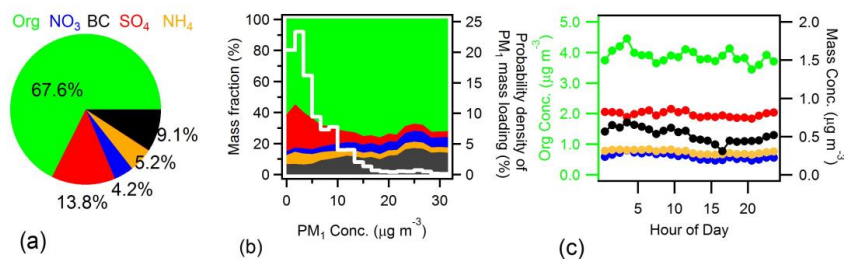
542

543

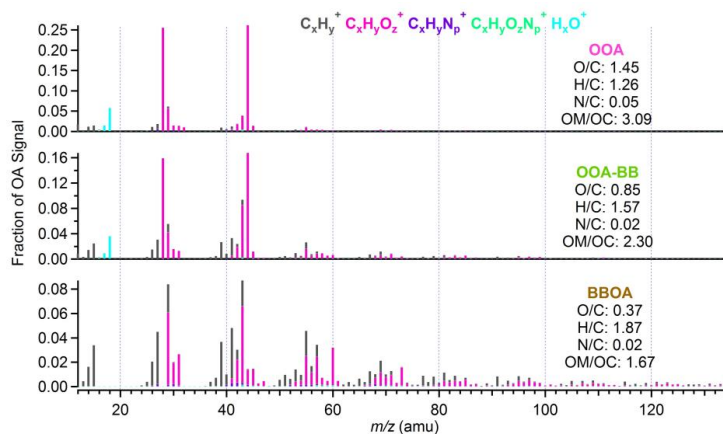
**Fig.1 The location of the sampling site at Mt. Yulong (27.2N 100.2E, 3410 m a.s.l.).**



544  
 545 **Fig.2** Time series of (a) relative humidity and temperature; (b) total mass concentrations from AMS plus  
 546 black carbon (c) mass fractions of different chemical species; (d) concentrations of black carbon and  $f_{60}$ . The  
 547 gray background denotes three biomass burning events (identified in Section 4.1).



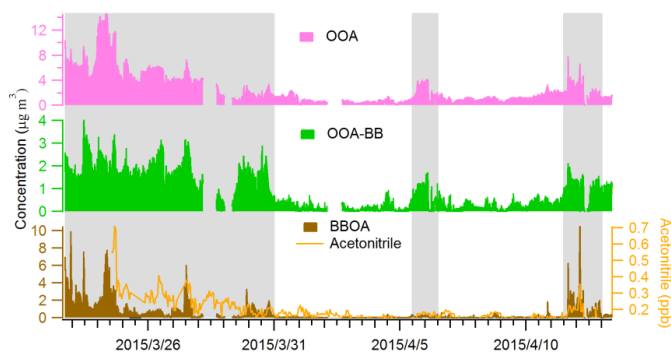
548  
 549 **Fig.3** (a) average chemical composition of the whole campaign; (b) the mass fractions of  $PM_{10}$  species as a  
 550 function of  $PM_{10}$  mass loading (left axis), with the white line representing the probability density of  $PM_{10}$  mass  
 551 loadings (right axis); (c) the diel cycle of different species, with the left axis for organics, and the right axis for  
 552 the rest components.



553

554

Fig.4 The mass spectra of each factor resolved by PMF, together with atomic ratios of each factor.



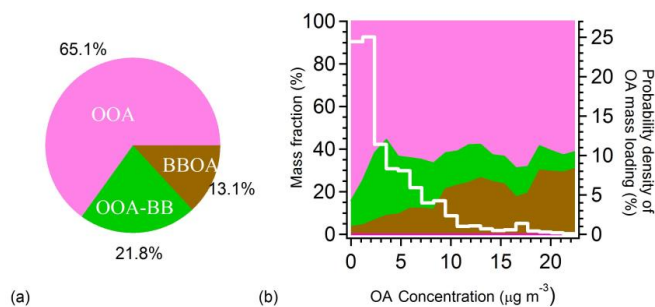
555

556

Fig.5 The time series of three OA factors resolved by PMF, together with acetone nitrile, a gas phase tracer for

557

biomass burning. The grey background areas denote the biomass burning events (identified in Section 4.1).



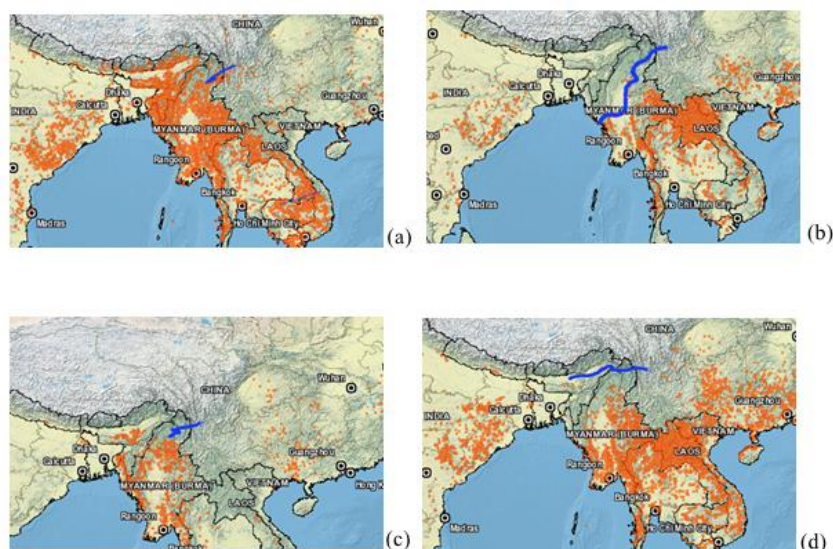
558

559

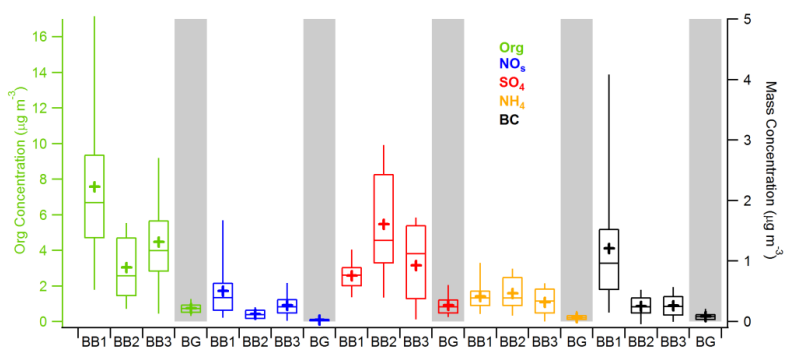
Fig.6 (a) contribution of each factor to the total OA mass; (b) fractions of OA factor (left axis) and

560

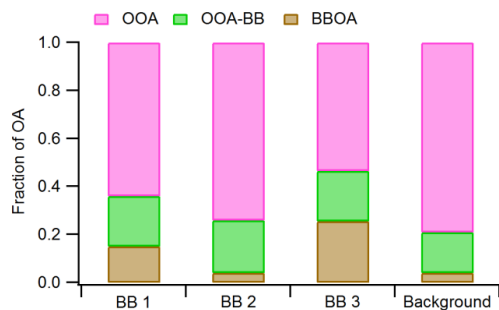
probability density of OA concentration (white line, right axis) as a function of OA mass loading.



561  
 562 **Fig.7 Occurrence of wildfire derived from MODIS images and back trajectories (blue lines) from WRF**  
 563 **model (a) first biomass burning event: March 22<sup>nd</sup> – 30<sup>th</sup>; (b) second biomass burning event: April 5<sup>th</sup> – 6<sup>th</sup>;**  
 564 **(c) third biomass burning event: April 11<sup>th</sup> – 12<sup>th</sup>; (d) background: April 1<sup>st</sup> – 4<sup>th</sup>.**  
 565

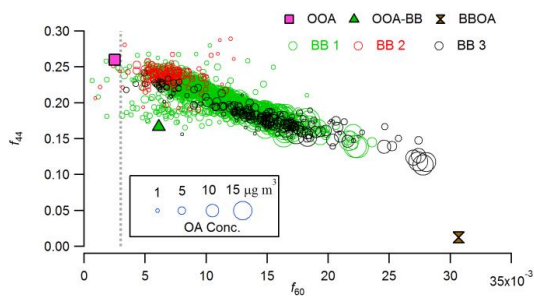


566  
 567 **Fig.8 Comparison of chemical compositions between three biomass burning events (BB1, BB2, BB3) and**  
 568 **background conditions (BG, highlighted by light gray color). Boxes denote median, 25th and 75th percentiles;**  
 569 **whiskers represent 5th and 95th percentiles; crosses represent mean values.**



570

571 **Fig.9 The relative contribution of different types of OA during three biomass burning events and**  
572 **background condition.**



573

574 **Fig.10  $f_{44}$  as a function of  $f_{60}$  ( $f_{44}$  vs.  $f_{60}$  triangle plot) of the three biomass burning events, sized by OA**  
575 **concentration.**